Science and Technology of Advanced Materials

ISSN: 1468-6996 (Print) 1878-5514 (Online) Journal homepage: www.tandfonline.com/journals/tsta20

Electron doping of exfoliated multilayer graphene induced by dissociative H_2 adsorption due to long-term exposure to 80-bar H_2 gas

Hyun-Seok Jang, Younghun Kim, Heewoo Lee, Soo Bong Choi, Jeongwoo Kim & Byung Hoon Kim

To cite this article: Hyun-Seok Jang, Younghun Kim, Heewoo Lee, Soo Bong Choi, Jeongwoo Kim & Byung Hoon Kim (05 Feb 2026): Electron doping of exfoliated multilayer graphene induced by dissociative H_2 adsorption due to long-term exposure to 80-bar H_2 gas, Science and Technology of Advanced Materials, DOI: 10.1080/14686996.2026.2627029

To link to this article: https://doi.org/10.1080/14686996.2026.2627029

Electron doping of exfoliated multilayer graphene induced by dissociative H_2 adsorption due to long-term exposure to 80-bar H_2 gas

Hyun-Seok Jang[a,b,‡], Younghun Kim[a,‡], Heewoo Lee[a,c], Soo Bong Choi[a,c], Jeongwoo Kim[a,c,*], and Byung Hoon Kim[a,c,d,*]

[a] *Department of Physics, Incheon National University, Incheon, 22012, Republic of Korea*

[b] *Strategic Research Center for Smart Battery, Korea Basic Science Institute, Daejeon, 34133, Republic of Korea*

[c] *Intelligent Sensor Convergence Research Center, Incheon National University, Incheon 22012, Republic of Korea*

[d] *Institute of Basic Science, Incheon National University, Incheon 22012, Republic of Korea*

*Jeongwoo Kim - Department of Physics, Incheon National University, Incheon, 22012, Republic of Korea; Intelligent Sensor Convergence Research Center, Incheon National University, Incheon, 22012, Republic of Korea; orcid.org/0000-0002-4070-1878; E-mail: kjwlou@inu.ac.kr

*Byung Hoon Kim – Department of Physics, Incheon National University, Incheon, 22012, Republic of Korea; Intelligent Sensor Convergence Research Center, Incheon National University, Incheon, 22012, Republic of Korea; Institute of Basic Science, Incheon National University, Incheon, 22012, Republic of Korea; orcid.org/0000-0003-1118-8590; E-mail: kbh37@inu.ac.kr

Electron doping of exfoliated multilayer graphene induced by dissociative H_2 adsorption due to long-term exposure to 80-bar H_2 gas

Semiconducting graphene is expected to replace silicon in the electronics industry, and various methods have been proposed for this purpose. In this study, we demonstrate that the long-term exposure of multilayer graphene to 80 bar of molecular hydrogen induces electron doping in graphene. Ambipolarity behavior disappeared, and the current in the transfer curves decreased and increased in the negative gate voltage (V_g) and positive V_g regions, respectively. The charge neutrality point shifted from 4.18 to over −80 V. Two resonant scatterings due to hydrogen adatoms were observed in the temperature-dependent transfer curves. For multilayer graphene with a boundary (edge), different behavior was observed in the transfer characteristics. Upon exposure to 80 bar of H_2 pressure, the drain current of the time-dependent transfer curve rapidly decreased; however, it increased in the positive V_g region after 60 h of exposure to H_2. Structural changes, particularly an increase in C–H bonding, were observed using various characterization methods. These results were interpreted by the dissociative H_2 adsorption of graphene. Molecular dynamics simulations also revealed the presence of electron doping due to dissociative adsorption. Furthermore, the simulations confirmed that dissociative adsorption occurred on the surface layer and at vacancies and defects.

Keywords: Multilayer graphene; High H_2 pressure; Dissociative H_2 adsorption; Hydrogen electron-doped graphene

Subject classification codes: include these here if the journal requires them

1. Introduction

Since the discovery of graphene, the electronics industry has regarded graphene as a substitute for silicon because of its remarkably high carrier mobility, transparency, high Young's modulus, and chiral half-integer quantum Hall effect [1-7]. Graphene also exhibits superconductivity [8] and has been used in various fields, such as light-emitting diodes, supercapacitors, photocatalysts, mechanical transduction, sensors, wearable electronics, energy storage, energy harvesting, tissue engineering, gene delivery, and biomedical sensors [9-14]. Although graphene exhibits these exotic properties, controlling the carrier types (*n*- and *p*-types) of graphene must proceed to replace the silicon industry.

Various methods have been proposed to control the carrier types of graphene. *p*-type graphene has been induced by functionalization with pyrenebutyric acid [15], cationic nitrogen doping [16], nitric acid doping [17], and optical excitation in organic and inorganic sandwich structures [18]. *n*-type graphene can be obtained using various methods, such as nitrogen [19-23] and potassium [24] doping, KBr doping under deep-ultraviolet (UV) irradiation [25], and functionalization with lanthanide complex [26], polyvinylpyrrolidone [15], and ion gel films [27]. Other methods include coating [28] and doping [29] of organic materials, hybridization with MoS_2 for *p*-*n* junction [30], heterostructure with carbon nanotubes [31] and ferroelectric $LiNbO_3$ crystals [32], organic and inorganic sandwich structures under UV [18], and atomic-layer deposition with water [33] and ozone [34]. However, these methods require the use of harmful chemicals or complicated procedures to change the electronic structure of graphene.

Exposure to high-pressure gas is a possible route for modifying the electronic structure of materials. For example, the oxidation of V^{4+}–V^{5+} of V_2O_5 nanowires due to

a CO_2 gas pressure of 45 bar has been reported [35]. High H_2 pressure induces electronic structural changes in MoS_2 [36-38], ZnO thin films [39], single-walled carbon nanotubes [40], and VO_2 nanowires [41]. For graphene, the dissociative H_2 adsorption has been considered a chemically unfavorable reaction. However, we previously reported that dissociative H_2 adsorption resulted in the shift of the charge neutrality point (CNP) toward the negative gate voltage (V_g) region due to 24-bar H_2 gas pressure at 300 K, and this behavior was enhanced at 345 K [42]. A temperature-dependent (from 300 K to 340 K) CNP shift from −2.0 to −10.5 V during 10-bar H_2 pressure was observed. The dissociative hydrogen atoms on multilayer graphene (MLG), resulting in C–H bonds, were measured by quartz crystal microbalance [43]. In addition, the proof of *n*-type doping of graphene due to high H_2 pressure has been reported [44-49]. However, the previous results mentioned above were achieved with relatively low pressure (maximum 24 bar H_2 gas) and short time (~500 min). Thus, the CNP shift was small, and ambipolarity was still observed after exposure to H_2.

In this study, we report the electron-doped MLG obtained by long-term exposure (762 h) to high-pressure H_2 gas (80-bar) to provide fundamental evidence for the enhancement of dissociative H_2 adsorption. The CNP shifted from 4.18 V in a vacuum to a negative V_g region and then vanished. The hole current was saturated. Finally, after 616 h, partially hydrogenated graphene (H-Gr) exhibited *n*-type semiconducting property under 80-bar H_2 at 300 K. Based on the current-voltage (*I*-*V*) characteristics, the electrical conductance (*G*) of graphene increased from 0.55 to 1.5 mS. The temperature-dependent transfer curve of H-Gr confirmed a resonant scattering due to the presence of hydrogen adatoms acting as scattering centers. The structural change was investigated by Raman spectroscopy, X-ray photoelectron spectroscopy (XPS), Fourier transform infrared spectroscopy (FT-IR), atomic force microscopy (AFM), and

X-ray diffraction (XRD). The ab initio molecular dynamics (MD) calculations, which demonstrated the dissociative H_2 adsorption of the graphene.

2. Materials and Methods

2.1. Sample Preparation

Mechanically exfoliated MLG obtained from highly oriented pyrolytic graphite (HOPG) flake (HQ graphene, Netherlands) for charge transport property measurement was deposited on 300-nm SiO_2/highly *p*-doped Si wafers (Figure S1a). The electrodes were patterned on the sample via e-beam lithography (JSM-6510, JEOL, Japan), followed by e-beam evaporation (TERA LEADER, Korea) of Cr/Au (5/50 nm). The sample was then wire-bonded to a PCB and loaded into the pressure chamber (Figure S1c). Structural changes were investigated using MLGs (Figure S2a–S2d) and bulk samples (Figure S2e–S2g) obtained from HOPG. The graphite powders (2–15 microns, 99,995%, Alfa Aesar, USA) were prepared for FT-IR measurements (Figure S2h).

2.2. Characteristics of Structural Change

The structural change of graphene induced by high-pressure gas exposure (after exposure to 80 bar H_2 pressure at 343 K for 150 h) was measured using FT-IR (VERTEX 80V, Bruker, USA), XRD (SmartLab, Rigaku, Japan) with Cu Kα radiation (λ = 1.5412 Å), XPS (PHI 5000 VersaProbe II, ULVAC-PHI, Japan), Raman spectroscopy (Raman-LTPL system, Witec alphy300, Witec, Germany) using 532-nm laser excitation, and AFM (XE-NSOM, Park systems, Korea).

2.3. Charge Transport Properties

I-V characteristics and transfer curves were measured using a semiconductor characterization system (4200-SCS, Keithley, USA) in a high-pressure stainless steel chamber. The devices were electrically characterized by a V_g sweep from –80 to 80 V with a drain-source bias of V_{ds} = 1.0 mV. First, the devices were loaded into the chamber, which was evacuated under 1.0×10^{-6} Torr at 300 K for 59 h and 325 K for 2 h. Second, the graphene sample was exposed to 99.999% H_2 gas at pressures ranging from vacuum to 80 bar in 5-bar intervals at 300 K. We waited for 30 min at each interval to obtain a stable pressure in the chamber before the measurement. Third, 80-bar H_2 pressure was maintained until G was saturated for 616 h. Fourth, H_2 gas was released by 5-bar intervals, and the devices were then exposed to ambient air at 300 K. Fifth, the same procedure was performed at 343 K. The temperature-dependent transfer characteristics before and after exposure to 80-bar H_2 gas pressure were measured in a cryostat (CH-202 10 K Cryocooler, Seongwoo Instruments, Korea).

2.4. Theoretical calculations

First-principles calculations were performed using *Quantum ESPRESSO* [50-52]. The Perdew–Burke–Ernzerhof functional of the generalized gradient approximation [53] was used to describe the exchange–correlation interactions among electrons, and Optimized Norm-Conserving Vanderbilt (ONCV) pseudopotentials [54] were used to describe the electron–ion interactions. The kinetic energy cutoff for the plane-wave basis set was set to 50 Ry. A self-consistent field convergence threshold of 10^{-6} Ry was applied. MD simulations were performed using a time step of 1.0 fs at a temperature of 300 K. The radial distribution functions (RDFs) [55] were averaged over 0.2 ps. Brillouin zone integrations were sampled using 2 × 7 × 5 and 2 × 7 × 1 Monkhorst–

Pack k-point grids [56] for stacked and monolayer graphene, respectively. A 4 × 2 rectangular supercell configuration under a hydrogen environment (16 atoms) was considered for hydrogenation simulation.

3. Results and Discussion

3.1. Conductance Change Due to High H_2 Pressure

Figure 1 shows the changes in *I-V* characteristics and *G* obtained from the linear fitting of *I-V* curves. The graphene was exposed to H_2 gas up to 80-bar by 5-bar intervals at 300 K (Figure S3a). *G* changed from 0.553 mS in a vacuum to 0.584 mS at 80-bar H_2 pressure. This value increased to 0.934 mS after 616 h in 80-bar H_2 pressure at 300 K (Figure 1a and 1b). As the pressure was released, *G* decreased to 0.911 mS (Figure S3b). After exposure to air, *G* decreased due to water or oxygen molecules and then saturated to 0.780 mS after 165 h (Figure 1c and 1d). Interestingly, the saturated *G* was larger than the *G* value in a vacuum (0.553 mS). The increase in *G* due to H_2 pressure can be interpreted as follows. Dissociative adsorption of hydrogen molecules on graphene breaks C=C double bonds, yielding two unpaired electrons. One of these unpaired electrons participates in the formation of a C–H bond, which disrupts the continuity of the π bond network, and the other electron is delocalized [57,58]. In addition, hydrogen adatoms donate electrons to the graphene [59]. Consequently, *G* increases [42]. Thermal energy accelerated this interaction. The graphene was loaded into the pressure chamber again, and the temperature of the chamber was then increased to 343 K in a high vacuum. The *G* value was recovered to 0.926 mS after 24 h in a vacuum, indicating the possibility of a reversible dissociative hydrogen adsorption process if the high temperature is applied. Figure 1e and 1f shows the dependence of *G*

on H_2 pressure at 343 K. The *G* increased from 0.926 mS in vacuum to 1.302 mS at 80 bar. As the exposure time increased at 80 bar, the *G* also increased up to 1.50 mS after 77 h and finally saturated until 146 h (Figure 1g and 1h). The effect of electron donation is clearly observed in the transfer characteristics because the additional electrons lead to *n*-type doping in graphene.

3.2. Transfer Characteristics Due to High H_2 Pressure

Figure 2a displays the change in transfer characteristics as a function of H_2 gas pressure up to 80 bar at 300 K. As the pressure increased, the currents in the positive and negative V_g regions increased and decreased, respectively. The CNP changed from 4.78 V in a vacuum to –6.61 V under 80-bar H_2 pressure (red arrow). In addition, in the time-dependent transfer curves at 80 bar, the CNP significantly shifted to –32.27 V at 96 h (Figure 2b) and –69.35 V at 514 h (Figure 2c). Finally, the CNP vanished after 585 h, and the transfer curve with a threshold voltage exhibited *n*-type semiconducting behavior. The plateau observed after 585 h at 300 K (Figure 2c) can be interpreted by the quantum phase cancellation between multi-scattering paths due to the disorders caused by hydrogen adatoms.

The pressure in the chamber was released from 80 to 5 bar after exposure to H_2 pressure for 616 h. The transfer curves were rarely changed (Figure 2d). Next, the sample was then exposed to air at 300 K. The broad CNP occurred again (Figure 2e). At a V_g value of 80 V, the current slightly decreased until 24 h; however, it increased after 52 h and was maintained until 180 h (Figure S4). Although the current level slightly decreases in the air, this result demonstrates that H-Gr remains stable in ambient conditions for at least 180 h. After the measurement of temperature-dependent transfer curves in a vacuum (1.0×10^{-6} Torr, it will be discussed later), the sample was reloaded

into the pressure chamber. As the chamber was held in a vacuum at 1.0×10^{-6} Torr and 343 K for 24 h, the CNP shifted to the negative V_g region, and the current in the positive V_g region increased (Figure 2f). Upon exposure to H_2 pressure at 343 K, the CNP shift and current increase were enhanced (Figure 2g). As the exposure time increased, the current was also augmented, and the CNP was shifted over –80 V, resulting in the realization of an electron-doped MLG using only H_2 gas (Figure 2h; changes in the CNP and mobility are summarized in Figure S5). The *n*-type behavior was also determined by the current of the four characteristic conditions as a function of the carrier density, *n* (Figure S6a). After 77 h of exposure to 80 bar of H_2 at 343 K, only the electron density existed and was 6×10^{12} cm^{-2} at $V_g = 0$ V (Figure S6b). Finally, high-pressure dependent electrical properties using one of the inert gases, He, were also measured to investigate the high-pressure effect (Figure S7). The result directly indicates that electron doping on MLG arises from the dissociative H_2 adsorption rather than from pressure effects.

3.3. Temperature-Dependent Charge Transport Behavior

Figure 3a shows the temperature-dependent resistance (R) of before (black circles) and after (pink circles) H_2 exposure measured at $V_g = 0$ V. The R of H-Gr is lower than that of pristine graphene. The R exhibited three distinct properties. First, the thermally activated process described by the Arrhenius expression at high temperatures (the blue dashed line), $R = R_0 \exp(E_A/k_B T)$, where E_A and k_B denote the activation energy and Boltzmann constant, respectively. Second, variable-range hopping in two-dimensional (2D) materials is expressed by $R = R_M \exp(T_M/T)^{1/3}$ in the middle temperature range. Third, saturation toward the Mott maximum resistance is observed at low temperatures (Figure S8). This behavior is similar to the trend previously reported on H-Gr [60]. The E_A values of pristine graphene and H-Gr are 12.3 and 9.51 meV, respectively. The small

E_A of H-Gr indicates that charge carriers are more easily activated from the chemical potential to the energy associated with the percolation paths. The Mott temperature, T_M, is inversely proportional to the density of states near the Fermi energy (E_F). The small T_M of H-Gr (269.8 K) compared to that of pristine graphene (406.6 K) showed a large density of states near E_F of H-Gr, as the theoretical calculation for low-concentration hydrogen of H-Gr [61].

Low temperatures can rule out thermal energy. Thus, the temperature-dependent transfer curves were measured down to 10 K. For pristine graphene, the current decreased as the temperature decreased, as expected (Figure 3b). The CNP slightly shifted to a negative V_g region (From 4.78 V at 300 K to 0.804 V at 10 K), which was caused by the high vacuum (1.0×10^{-6} Torr). The temperature-dependent transfer curves of H-Gr were measured in a vacuum after 180 h of exposure to air (Figure S4). At 300 K, *n*-type characteristics and two broad peaks near –10 and –60 V were observed (Figure 3c). The peak at –60 V originated from the CNP shift, whereas the peak at –10 V resulted from the resonance scattering of the dimer, which was shifted to –20 V with decreasing temperature (red arrow). Another peak at 13.2V emerged from 60 K and was visible at 10 K (blue arrow). This can be attributed to the resonance scattering of the β sublattice. The interpretation of the resonance scattering occurred due to hydrogen atom is as follows: Hydrogen adatoms (defects) create a localized state with narrow energy width near Dirac point, acting as the resonant scatterers. J. Katoch et al. observed two distinct resonant peaks appear in the V_g-dependent resistance of H-Gr, akin to those shown in Figure 3c. They determined that both peaks are associated with hydrogen adatoms located on different graphene sublattices and also calculated the density of state for resonant defect levels of hydrogen. The energy level for the α sublattice (dimer site) is closer to CNP than that for the β sublattice (non-dimer site) [59]. This finding is

consistent with the V_g-dependent drain current observed in this study. The small fluctuation of current at low temperatures in both samples is caused by the interference of electrons scattered from a distribution of scattering centers [62]. These results indicate dissociative H_2 adsorption behavior. The electrical properties of MLG provide evidence of dissociative H_2 adsorption on MLG, resulting in electron doping that is further enhanced by prolonged exposure to high H_2 pressure.

3.4. Structural Change after H_2 Exposure

Figure 4a and 4b shows the FT-IR results of graphite powder before and after exposure to 80 bar H_2 gas. Before H_2 exposure (Pristine), oxygen-related modes were observed at 1101 (C–O–C), 1251, 1353 (stretching mode of C–O), 1371 (bending of C–OH), and 1504 cm^{-1} (O–C–O bending vibration) (pink indices in Figure 4a). In contrast, in H-Gr, the modes at 1101, 1251, 1504 cm^{-1} disappeared, whereas those at 1353 and 1371 cm^{-1} weakened (blue line in Figure 4a). The C–H bending mode was observed at 1454 cm^{-1} in pristine graphite. However, the additional stretching and bending vibrations of C–H at 1270, 1317, 1396, 1419, 1473, and 1522 cm^{-1} were observed (blue indices) in H-Gr [63]. Vibration modes over 1530 cm^{-1} are relevant to C=C bonds. The modes at 1533 and 1540 cm^{-1} can be designated by sp^2 C=C bonds. The peaks at 1600 – 1580 cm^{-1} in pristine graphite correspond to the stretching vibrations of the aromatic C=C bond. These modes were relatively weakened in H-Gr, indicating that some aromatic structures were broken due to H_2 gas. The enhancement of C–H vibration was found in H-Gr at high wavenumbers (Figure 4b). In pristine graphite, symmetrical stretching in-phase C–H bonds (SSI, 2862 cm^{-1}), asymmetrical stretching out-of-plane C–H bonds from methylene (ASOM, 2923 cm^{-1}), and asymmetrical stretching out-of-plane C–H bonds from methyl (2958 cm^{-1}) were observed [63]. An increase in the transmittance intensity of SSI and ASOM was shown in H-Gr. In addition, a new broad

peak was observed at 3004 cm^{-1} in H-Gr. This mode corresponds to sp^2 C–H bonds [63]. The O–H vibration near 3238 cm^{-1} in pristine graphite was indiscernible in H-Gr. According to the FT-IR results, upon H_2 exposure, oxygen bonds with carbon atoms are lost, whereas C–H bonds are created and enhanced.

The (002), (004), (100), and (101) peaks are the representative planes in HOPG (Figure 4c and 4d). Shift to small angles occurred in (002), (004), and (101) peaks in H-Gr. The *d*-spacings increased from 3.356 to 3.363 Å for the (002) plane, from 1.678 to 1.680 Å for the (004) plane (Figure 4c), and from 2.031 to 2.037 Å for the (101) plane (Figure 4d). The structural changes are 0.21%, 0.12%, and 0.30% for the (002), (004), and (101) planes, respectively. The (100) peak was significantly reduced; however, the (101) peak became protuberant after exposure to H_2 gas (Figure 4d). The symmetry of the (100) plane was weakened, whereas that of the (101) plane was relatively enhanced. This can be attributed to the energetically favorable resonance scattering of the β sublattice, i.e., the dissociative hydrogen adsorbs preferentially onto the edge and defect sites and the β sublattice related to the (100) plane [59].

To evaluate the structural impact of high-pressure hydrogen exposure, Raman spectra were collected from eight distinct locations across four samples. **Figure 4e** displays a representative optical image of the few-layer graphene used for this analysis. In pristine graphene, a sharp *G* band was observed at approximately 1576 cm^{-1}. Following H_2 exposure, a broad *D* peak emerged (Figure 4f and Figure S9), indicating the formation of sp^3 defects. Additionally, the averaged position of the *G* peak exhibited a blue-shifted from 1576.4 ± 1.3 cm^{-1} in pristine graphene to 1579.2 ± 1.7 cm^{-1} in the H-Gr (Figure 4g). The second-order resonance (*2D* band) of pristine graphene is characterized by three constituent peaks located near 2640 (*D1*), 2690 (*D2*), and 2718 cm^{-1} (*D3*) (Figure 4h). While the *D1* peak was barely discernible in pristine graphene, this defect-

originated peak became prominent in H-Gr. The *D2* and *D3* peaks correspond to 2- and 3-dimensional graphitic structures, respectively [64,65]. The intensification of the *D2* band of H-Gr is attributed to a reduction in the stacking order and an increase in the structural strain induced by the presence of hydrogen adatoms. Interestingly, while defect-related features were identified in the *2D* band of the MLG surface, the *D* band remained absent both before and after exposure to high-pressure H_2 (Figure S10). This indicates that hydrogenation-induced defects are predominantly concentrated at domain boundaries and edges (Figure 4e and Figure S9).

XPS analyses of HOPG before and after exposure to H_2 pressure were performed. The C1s peak was composed of sp^2, sp^3, C–O, C=O, and π–π* shake-up feature, which were attributed to the aromatic structure of the benzene ring (Figure S11a and S11b). The amounts of all species except the sp^3 bonds, decreased in H-Gr. In other words, the amount of sp^3 bonds increased from 31.26% to 36.19% (Table S1). This is due to an increase in the number of C–H bonds. The oxygen species (O–H, C–O, and C=O) in the O1s peak were also reduced after H_2 exposure (Figure S11c and S11d, Table S1). Since sp^3 bonding is considered a direct indicator for C–H covalent bond formation, we focused on the 4.93% increase in sp^3 bonds after exposure to H_2. This corresponds with the obtained electron carrier density from the transfer curve, -5.52×10^{12} cm^{-2} (Figure S12). Although meaningful structural changes were observed in the FT-IR, Raman spectroscopy, and XPS results, the change in height obtained from AFM was small but highly consistent with the XRD results, showing an increase of 0.195-0.207%. (Figure S13).

3.5. Comparison of Dissociative H_2 Adsorption between Edge and Surface

At the edges and vacancy defects in graphite, the dissociative energy barrier of H_2 is

reduced [66-68], as observed in Raman spectroscopy. We prepared an MLG separated into two parts, one part has an even surface (s-MLG, blue circle in Figure S14a and S14b) and the other part has a boundary (white circle in Figure S14a and S14c), to compare the edge and surface effects of graphene and to confirm reproducibility of electron doping on MLG. A 2.17-nm height difference was observed in the MLG with a boundary (MLG-b) using AFM (Figure S14c). Under 80-bar H_2 pressure, the time-dependent (from 0 h to 528 h) transfer characteristics of s-MLG at 300 K are similar to those shown in Figure 2 (**Figure 5**a). For MLG-b, a different behavior is observed. The drain current in the transfer curve decreased upon exposure to 80 bar of H_2 until 60 h (green arrow in Figure 5b), indicating that gap-opening occurred rapidly because dissociative hydrogen atoms acting as defects were first adsorbed at the boundary (edge). After 60 h of exposure, the current due to electrons (the positive V_g region) monotonously increased (pink arrow). However, the hole current (blue arrow) continuously decreased until 352 h and then slightly increased, finally it was saturated. This is attributed to competition between the surplus electrons and attached hydrogen atoms on and into the MLG layers after dissociation. The surplus electrons had a dominant effect after 60 h. Figure 5c shows that the variation in CNP per volume of MLG-b from 0 to 528 h is larger (137.51 V/μm^3) than that of s-MLG (114.93 V/μm^3). This proves that the potential barrier for H_2 dissociation is smaller at the edges than at the surface of graphene. The dissociative H_2 adsorption was confirmed via a MD simulations.

3.6. Theoretical Evidence for Dissociative H_2 Adsorption

To investigate the adsorption behavior of hydrogen atoms on graphite, we performed *ab initio* MD simulations. Because pristine graphite is generally inert toward hydrogen adsorption, we considered representative defect structures commonly observed in

graphite —specifically, a single vacancy (**Figure 6**a) and 5–7 defects (Figure 6b)—to simulate the dissociation of hydrogen molecules and the subsequent adsorption process. The calculated RDF reveals that hydrogen atoms are preferentially absorbed in the vicinity of these defect sites (Figure 6c and 6d). Remarkably, hydrogen adsorption was also observed on the pristine, defect=free graphene layer, as indicated by the black curves in Figure 6c and 6d. During the hydrogen dissociation process, one hydrogen atom from the molecule is attracted to the defect site, while the other forms a chemical bond with a neighboring graphene layers (Figure 6e, 6f and Movie S1, Movie S2). These observations demonstrate that, contrary to conventional expectation, a substantial number of hydrogen atoms were adsorbed not only at the defect sites but also on the pristine graphene layers.

The charge density variation and the average energy of occupied carbon states were also calculated to investigate charge transfer during the hydrogenation process (Figure 6g). In all structures considered—the pristine, the vacancy, and the 5–7 defect layers—carbon atoms gain electrons from adsorbed hydrogen atoms, confirming that hydrogenation results in *n*-type doping. Correspondingly, the average energy of the occupied carbon states shifts downward, consistent with charge transfer from hydrogen to carbon atoms during the hydrogenation process.

4. Conclusion

Upon long-term exposure of MLG to 80 bar of hydrogen molecules, electron doping on MLG was investigated using *I-V* and transfer characteristics. As the H_2 pressure increased at 300 K, the *G* increased, and the current of the transfer curves decreased and increased in the negative V_g and positive V_g regions, respectively. The CNP also shifted

to the negative V_g region. These behaviors were enhanced in the time-dependent transfer curves at a H_2 pressure of 80 bar at 343 K, after which the CNP disappeared. At 300 K, the comparison of the time-dependent transfer curves between s-MLG and MLG-b at 80 bar of H_2 shows that the potential barrier for H_2 dissociation is smaller in MLG-b than in s-MLG. Two dips were observed in temperature-dependent transfer curves of H-Gr, resulting from the resonance scattering of the β sublattice due to hydrogen adatoms. The structural change of H-Gr was demonstrated using FT-IR, Raman spectroscopy, XPS, and XRD analyses. The dissociative adsorption of H_2 molecules in MLG was also investigated using ab initio MD simulations, which were well consistent with the experimental results.

Acknowledgements

The authors would like to thank Minseo Kim, Jaewoo Shin, and Yunhyeog Lee for the laboratory technical support. This work was supported by the Incheon National University Research Grant in 2024-0036, and the National Research Council of Science & Technology (NST) grant by the Korean Government (MSIT) (No. GTL25091-000).

Disclosure Statement

No potential conflict of interest was reported by the authors.

Funding

This work was supported by the Incheon National University Research Grant in 2024-

0036, and the National Research Council of Science & Technology (NST) grant by the Korean Government (MSIT) (No. GTL25091-000).

CrediT Authorship Contribution Statement

Hyun-Seok Jang: Conceptualization, Data curation, Methodology, Investigation, Formal analysis, and Writing-original draft. **Younghun Kim:** Methodology, Data curation, Formal analysis, Investigation, and Writing-original draft. **Heewoo Lee:** Methodology and Investigation. **Soo Bong Choi:** Methodology and Investigation. **Jeongwoo Kim:** Writing-original draft, Data curation, Methodology, Review, Editing and supervision. **Byung Hoon Kim:** Conceptualization, Methodology, Formal anaysis, Data curation, Writing-original draft, Review, Editing, Supervision, and Funding acquisition.

[‡] Hyun-Seok Jang and Younghun Kim contributed equally to this work

Data Availability Statement

The data that support the findings of this study are available from the corresponding author upon reasonable request.

References

[1] Novoselov K. S, Geim A. K, Morozov S. V, et al. Electric field effect in atomically thin carbon films. Science. 2004;306(5696):666-669. doi: 10.1126/science.1102896

[2] Zhang Y, Tan Y.-W, Stormer H. L, et al. Experimental observation of the quantum Hall effect and Berry's phase in graphene. Nature. 2005;438(7065):201–204. doi: 10.1038/nature04235

[3] Geim A. K, Novoselov K. S. The rise of graphene. Nat Mater. 2007;6(3):183-191. doi: 10.1038/nmat1849

[4] Lee C, Wei X, Kysar J. W, et al. Measurement of the elastic properties and intrinsic strength of monolayer graphene. Science. 2008;321(5887):385-388. doi: 10.1126/science.1157996

[5] Nomura K, MacDonald A. H. Quantum transport of massless Dirac fermions. Phys Rev Lett. 2007;98(7):076602. doi: 10.1103/PhysRevLett.98.076602

[6] Banszerus L, Schmitz M, Engels S, et al. Ultrahigh-mobility graphene devices from chemical vapor deposition on reusable copper. Sci Adv. 2015;1(6):e1500222. doi: 10.1126/sciadv.1500222

[7] Tyagi A, Mišeikis V, Martini L, et al. Ultra-clean high-mobility graphene on technologically relevant substrates. Nanoscale. 2022;14(6):2167-2176. doi: 10.1039/D1NR05904A

[8] Cao Y, Fatemi V, Fang S, et al. Unconventional superconductivity in magic-angle graphene superlattices. Nature. 2018;556(7699):43-50. doi: 10.1038/nature26160

[9] Dhinakaran V, Stalin B, Swapna Sai M, et al. Recent developments of graphene composites for energy storage devices. Mater Today Proc. 2021;45:1779-1782. doi: 10.1016/j.matpr.2020.08.631

[10] Olabi A. G, Abdelkareem M. A, Wilberforce T, et al. Application of graphene in energy storage device - A review. Renewable Sustainable Energy Rev. 2021;135:110026. doi: 10.1016/j.rser.2020.110026

[11] Carvalho A. F, Kulyk B, Fernandes A. J. S, et al. A review on the applications of graphene in mechanical transduction. Adv Mater. 2022;34(8):2101326. doi: 10.1002/adma.202101326

[12] Yang Y, Yan W, Anand A, et al. 3D N-doped crumpled graphene aerogels for thermoelectric energy harvesting and highly sensitive piezoresistive sensing. Carbon 2025;232:119827. doi: 10.1016/j.carbon.2024.119827

[13] Huang Z, Wang Z, Bi X, et al. B, N, O, S heteroatom-doped laser-induced porous lignin-derived graphene for stretchable rubber-based supercapacitors. J. Energy Storage 2025;116:116095. doi: 10.1016/j.est.2025.116095

[14] Sun M, Wang S, Liang Y, et al. Flexible graphene field-effect transistors and their application in flexible biomedical sensing. Nano-Micro Lett. 2025;17:34. doi: 10.1007/s40820-024-01534-x

[15] Novak T. G, Kim J, Kim J, et al. Complementary n-type and p-type graphene films for high power factor thermoelectric generators. Adv Funct Mater. 2020;30(28):2001760. doi: 10.1002/adfm.202001760

[16] Chae S, Panomsuwan G, Bratescu M. A, et al. p-type doping of graphene with cationic nitrogen. ACS Appl Nano Mater. 2019;2(3):1350-1355. doi: 10.1021/acsanm.8b02237

[17] D'Arsié L, Esconjauregui S, Weatherup R. S, et al. Stable, efficient p-type doping of graphene by nitric acid. RSC Adv. 2016;6(114):113185-113192. doi: 10.1039/c6ra23727d

[18] Ho P.-H, Li S.-S, Liou Y.-T, et al. Wavelength-selective dual p- and n-type carrier transport of an organic/graphene/inorganic heterostructure. Adv Mater. 2015;27(2):282-287. doi: 10.1002/adma.201403694

[19] Wang X, Li X, Zhang L, et al. N-doping of graphene through electrothermal reactions with ammonia Science. 2009;324(5928):768-771. doi: 10.1126/science.1170335

[20] Zhao L, He R, Rim K. T, et al. Visualizing individual nitrogen dopants in monolayer graphene. Science. 2011;333(6045):999-1003. doi: 10.1126/science.120875

[21] Bie C, Yu H, Cheng B, et al. Design, fabrication, and mechanism of nitrogen-doped graphene-based photocatalyst. Adv Mater. 2021;33(9):2003521. doi: 10.1002/adma.202003521

[22] He B, ren Z, Qi C, et al. Synthesis of nitrogen-doped monolayer graphene with high transparent and n-type electrical properties. J Mater Chem C. 2015;3(24):6172-6177. doi: 10.1039/c5tc01046b

[23] Yang J, He W, Jiang Q, et al. Hydrogen-dominated metal-free growth of graphitic-nitrogen doped graphene with n-type transport behaviors. Carbon. 2020;161:123-131. doi: 10.1016/j.carbon.2020.01.051

[24] Yamada T, Okigawa Y, Hasegawa M. Potassium-doped n-type bilayer graphene. Appl Phys Lett. 2018;112(4):043105. doi: 10.1063/1.5012808

[25] Khan M. F, Elahi E, Hassan N. U, et al. Bipolar photoresponse of a graphene field-effect transistor induced by photochemical reactions. ACS Appl Electron Mater. 2023;5(9):5111-5119. doi: 10.1021/acsaelm.3c00851

[26] Gajarushi A. S, Wasim M, Nabi R, et al. Lanthanide complexes as molecular dopants for realizing air-stable n-type graphene logic inverters with symmetric transconductance. Mater Horiz. 2019;6(4):743-750. doi: 10.1039/c8mh01241e

[27] Kanahashi K, Ishihara M, Hasegawa M, et al. Giant power factors in p- and n-type large-area graphene films on a flexible plastic substrate. npj 2D Mater Appl. 2019;3(1):44. doi: 10.1038/s41699-019-0128-0

[28] Kim S, Zhao P, Aikawa S, et al. Highly stable and tunable n-type graphene field-effect transistors with poly(vinyl alcohol) Films. ACS Appl Mater Interfaces. 2015;7(18):9702-9708. doi: 10.1021/acsami.5b01474

[29] Jo I, Kim Y, Moon J, et al. Stable n-type doping of graphene via high-molecular-weight ethylene amines. Phys Chem Chem Phys. 2015;17(44):29492-29495. doi: 10.1039/c5cp03196f

[30] Meng J, Song H.-D, Li C.-Z, et al. Lateral graphene p-n junctions formed by the graphene/MoS_2 hybrid interface. Nanoscale. 2015;7(27):11611-11619. doi: 10.1039/c5nr02552d

[31] Xiao M, Lin Y, Xu L, et al. n-type Dirac-source field-effect transistors based on a graphene/carbon nanotube heterojunction. Adv Electron Mater. 2020;6(7):2000258. doi: 10.1002/aelm.202000258

[32] Xiong Z, Meng S, Ma X, et al. Dramatic n-type doping of monolayer graphene with ferroelectric $LiNbO_3$ crystals and bilayer two-dimensional electron gases. J Phys Chem C. 2022;126(9):4534-4541. doi: 10.1021/acs.jpcc.1c10856

[33] Zheng L, Cheng X, Wang Z, et al. Reversible n-type doping of graphene by H_2O-based atomic-layer deposition and its doping mechanism. J Phys Chem C. 2015;119(11):5995-6000. doi: 10.1021/jp511562t

[34] Peng S, Jin Z, Yao Y, et al. Controllable p-to-n type conductance transition in top-gated graphene field effect transistor by interface trap engineering. Adv Electron Mater. 2020;6(9):2000469. doi: 10.1002/aelm.202000496

[35] Jang H.-S, Lee C. Y, Jeon J. W, et al. Interaction between V_2O_5 nanowires and high pressure CO_2 gas up to 45 bar: electrical and structural Study. J Adv Res. 2020;24:205-209. doi: 10.1016/j.jare.2020.01.014

[36] Jang H.-S, Kim T. H, Kim T. H, et al. Effect of high H_2 pressure on the structural and the electrical properties of MoS_2. J Korean Phys Soc. 2021;79(1):38-43. doi: 10.1007/s40042-021-00181-4

[37] Cho S, Kim B. S, Kim B, et al. Electronic-dimensionality reduction of bulk MoS_2 by hydrogen treatment. Phys Chem Chem Phys. 2018;20(35):23007-23012. doi: 10.1039/c8cp02365d

[38] Kim B. H, Park M, Lee M, et al. Effect of sulphur vacancy on geometric and electronic structure of MoS_2 induced by molecular hydrogen treatment at room temperature. RSC Adv. 2013;3(40):18424-18429. doi: 10.1039/C3RA42072H

[39] Chu H, Kim B. H, Kang J. Electrical transport property of ZnO thin films at high H_2 pressures up to 20 bar. J Korean Phys Soc. 2016;69(3):277-281. doi: 10.3938/jkps.69.277

[40] Kang H, Hong S. J, Park M, et al. Tuning the electronic structure of single-walled carbon nanotube by high-pressure H_2 exposure. Nanotechnology. 2018;30(6):065201. doi: 10.1088/1361-6528/aaf12b

[41] Kim J.-E, Shin J. Y, Jang H.-S, et al. Influence of hydrogen incorporation on conductivity and work function of VO_2 nanowires. Nanoscale. 2018;11(10):4219-4225. doi: 10.1039/C9NR00245F

[42] Kim B. H, Hong S. J, Baek S. J, et al. N-type graphene induced by dissociative H_2 adsorption at room temperature. Sci Rep. 2012;2(1):690. doi: 10.1038/srep00690

[43] Shin D. S, Kim Y. B, Kim D. Y, et al. Direct measurement of the amount of dissociated hydrogen atoms attached on graphene. Synth Met. 2015;200:80-84. doi: 10.1016/j.synthmet.2014.12.032

[44] Park M, Yun Y. J, Lee M, et al. Local doping of graphene devices by selective hydrogen adsorption. AIP Adv. 2015;5(1):017120. doi: 10.1063/1.4906254

[45] Hong S. J, Park M, Kang H, et al. Verification of electron doping in single-layer graphene due to H_2 exposure with thermoelectric power. Appl Phys Lett. 2015;106(14):142110. doi: 10.1063/1.4917470

[46] Hong S. J, Kang H, Park M, et al. Competition between electron doping and short-range scattering in hydrogenated bilayer graphene on hexagonal boron nitride. RSC Adv. 2015;5(125):103276-103279. doi: 10.1039/C5RA18945D

[47] Kim J, Kwak C. H, Jung W, et al. Variation in the c-axis conductivity of multi-layer graphene due to H_2 exposure. Phys Chem Chem Phys. 2016;18(23):15514-15518. doi: 10.1039/C6CP01745B

[48] Hong S. J, Park M, Kang H, et al. Manipulation of electrical properties in CVD-grown twisted bilayer graphene induced by dissociative hydrogen adsorption. Curr Appl Phys. 2016;16(12):1637-1641. doi: 10.1016/j.cap.2016.09.019

[49] Hong S. J, Kim H, Lee M, et al. Chemical manipulation of edge-contact and encapsulated graphene by dissociated hydrogen adsorption. RSC Adv. 2017;7(10):6013-6017. doi: 10.1039/C6RA26853F

[50] Giannozzi P, Baroni S, Bonini N, et al. Quantum espresso: a modular and open-source software project for quantum simulations of materials. J Phys: Condens Matter. 2009;21(39):395502. doi: 10.1088/0953-8984/21/39/395502

[51] Giannozzi P, Andreussi O, Brumme T, et al. Advanced capabilities for materials modelling with quantum espresso. J Phys: Condens Matter. 2017;29(46):465901. doi: 10.1088/1361-648X/aa8f79

[52] Giannozzi P, Baseggio O, Bonfà P, et al. Quantum espresso toward the exascale. J Chem Phys. 2020;152(15):154105. doi: 10.1063/5.0005082

[53] Perdew J. P, Burke K, Ernzerhof M. Generalized gradient approximation made simple. Phys Rev Lett. 1996;77(18):3865. doi: 10.1103/PhysRevLett.77.3865

[54] Hamann D. R. Optimized norm-conserving Vanderbilt pseudopotentials. Phys Rev B. 2013;88(8):085117. doi: 10.1103/PhysRevB.88.085117

[55] Jang H.-S, Kim S, Park I, et al. Long-range ordered graphitic structure in silk fibers delaminated using dopamine and thermal treatment for super-flexible electronic textiles: Possible applications for magnetic and thermoelectric textiles. Adv Compos Hybrid Mater. 2024;7(2):37. doi: 10.1007/s42114-024-00857-y

[56] Monkhorst H. J, Pack J. D. Special points for Brillouin-zone integrations. Phys Rev B. 1976;13(12):5188. doi: 10.1103/PhysRevB.13.5188

[57] Boukhvalov D. W, Katsnelson M. I, Lichtenstein A. I. Hydrogen on graphene: electronic structure, total energy, structural distortions and magnetism from first principles calculations. Phys Rev B. 2008;77(3):035427. doi: 10.1103/PhysRevB.77.035427

[58] Brenner K, Yang Y, Murali R. Edge doping of graphene sheets. Carbon. 2012;50(2):637-645. doi: 10.1016/j.carbon.2011.09.021

[59] Katoch J, Zhu T, Kochan D, et al. Transport spectroscopy of sublattce-resolved resonant scattering in hydrogen-doped bilayer graphene. Phys Rev Lett. 2018;121(13):136801. doi: 10.1103/PhysRevLett.121.136801

[60] Son J, Lee S, Kim S. J, et al. Hydrogenated monolayer graphene with reversible and tunable wide band gap and its field-effect transistor. Nat Commun. 2016;7(1):13261. doi: 10.1038/ncomms13261

[61] Huang H.-C, Lin S.-Y, Wu C.-L, et al. Configuration- and concentration-dependent electronic properties of hydrogenated graphene. Carbon. 2016;103:84-93. doi: 10.1016/j.carbon.2016.02.061

[62] Skákalová V, Kaiser A. B, Yoo J. S, et al. Correlation between resistance fluctuations and temperature dependence of conductivity in graphene. Phys Rev B. 2009;80(15):153404. doi: 10.1103/PhysRevB.80.153404

[63] Tucureanu V, Matei A, Avram A. M. FTIR spectroscopy for carbon family study. Crit Rev Anal Chem. 2016;46(6):502-520. doi: 10.1080/10408347.2016.1157013

[64] Pimenta M. A, Dresselhaus G, Dresselhaus M. S, et al. Studying disorder in graphite-based systems by Raman spectroscopy. Phys Chem Chem Phys. 2007;9(11):1276-1290. doi: 10.1039/B613962K

[65] Barros E. B, Demir N. S, Souza Filho A. G, et al. Raman spectroscopy of graphitic foams. Phys Rev B. 2005;71(16):165422. doi: 10.1103/PhysRevB.71.165422

[66] Allouche A, Ferro Y. Dissociative adsorption of small molecules at vacancies on the graphite (0001) surface. Carbon. 2006;44(15):3320–3327. doi: 10.1016/j.carbon.2006.06.014

[67] Diño W. A, Miura Y, Nakanishi H, et al. H_2 dissociative adsorption at the armchair edges of graphite. Solid State Commun. 2004;132(10):713–718. doi: 10.1016/j.ssc.2004.08.043

[68] Sha X, Jackson B. The location of adsorbed hydrogen in graphite nanostructures. J Am Chem Soc. 2004;126(40):13095–13099. doi: 10.1021/ja0472836

Figures

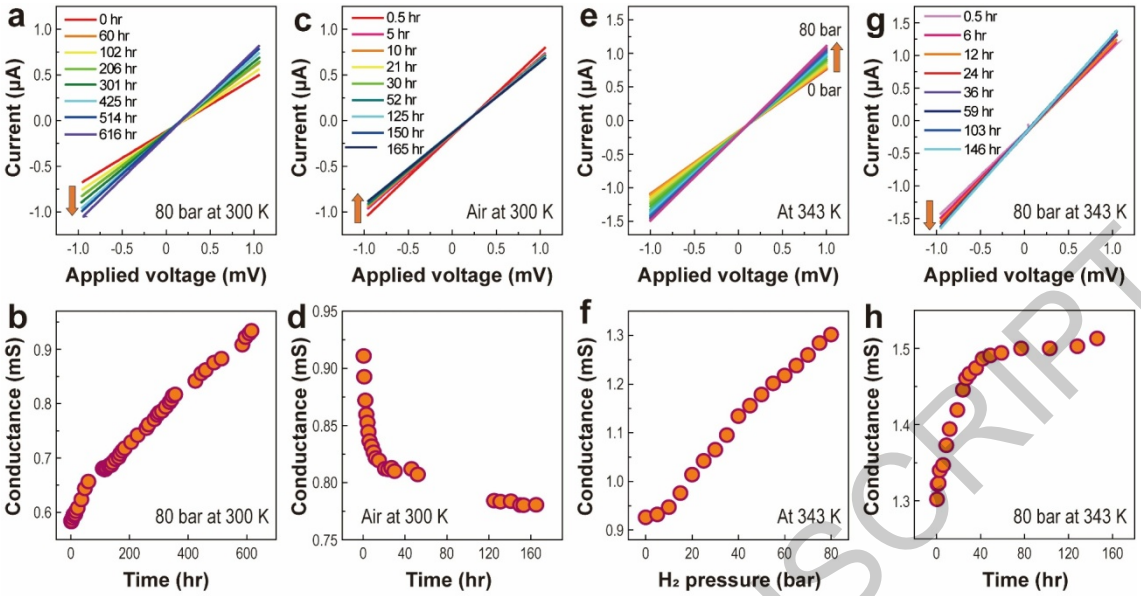

Figure 1. *I-V* characteristics and *G* of the MLG. The *G* was obtained from the *I-V* curve. (a) Time-dependent *I-V* curves and (b) *G* under 80 bar H_2 gas pressure at 300 K. (c) Time-dependent *I-V* curves and (d) *G* in air at 300 K, showing that *G* nearly saturated after 120 h. (e) H_2 pressure-dependent (from vacuum to 80 bar) *I-V* characteristics and (f) *G* at 343 K. (g) Time-dependent *I-V* curve and (h) *G* under 80-bar H_2 gas pressure at 343 K.

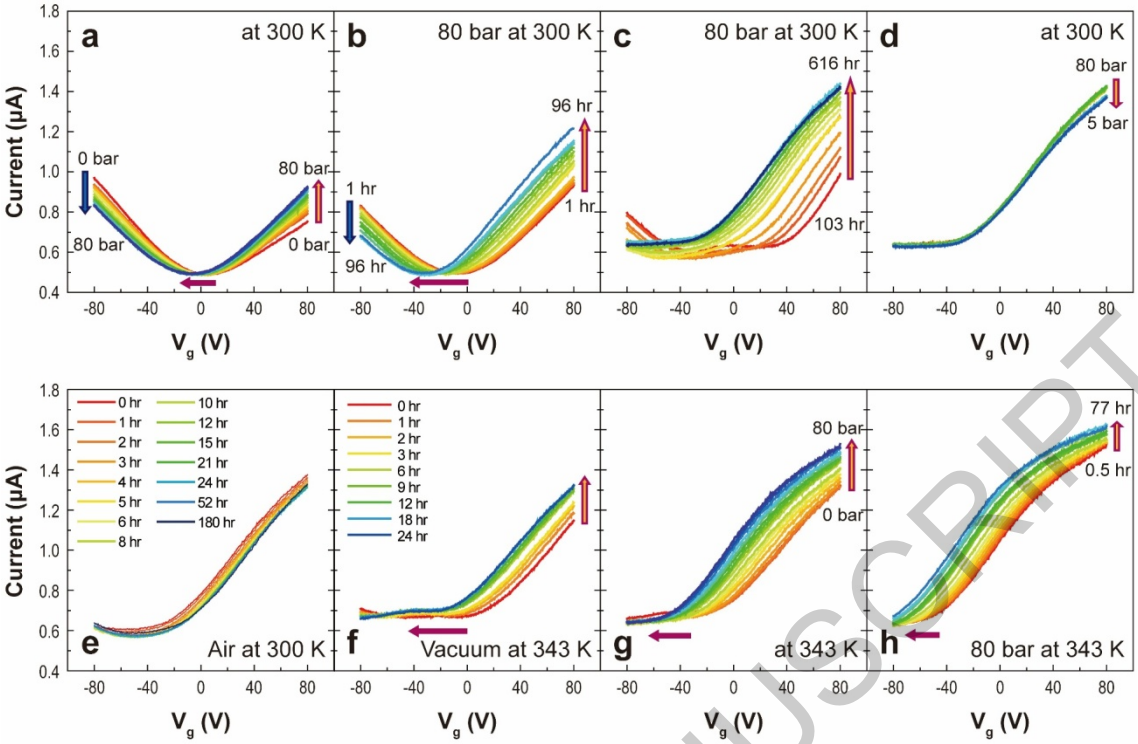

Figure 2. H_2 pressure- and time-dependent transfer curves of the MLG. The red horizontal arrows represent the CNP (or threshold voltage) shift. (a) H_2 pressure-dependent transfer curves at 300 K. (b) Time-dependent transfer curves from 1 to 96 h and (c) to 616 h under 80-bar H_2 at 300 K. (d) Transfer curves during the release of H_2 pressure at 300 K. (e) Time-dependent transfer curves under exposure to air at 300 K. (f) Time-dependent transfer curves in a high vacuum at 343 K from 0 to 24 h. (g) H_2 pressure-dependent transfer curves from vacuum to 80-bar H_2 at 343 K. (h) Time-dependent transfer curves under 80-bar H_2 at 343 K

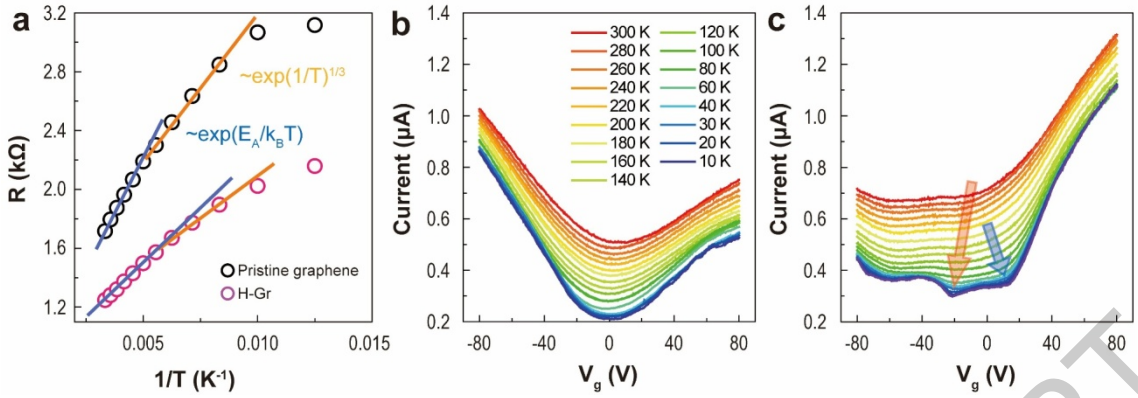

Figure 3. Temperature-dependent electrical transport properties of the MLG. (a) Temperature-dependent R at $V_g = 0$ V, accompanied by fitting results using different charge transport models, including the Arrhenius model and variable-range hopping. (b) Temperature-dependent transfer curves of pristine graphene. (c) Temperature-dependent transfer curves of H-Gr

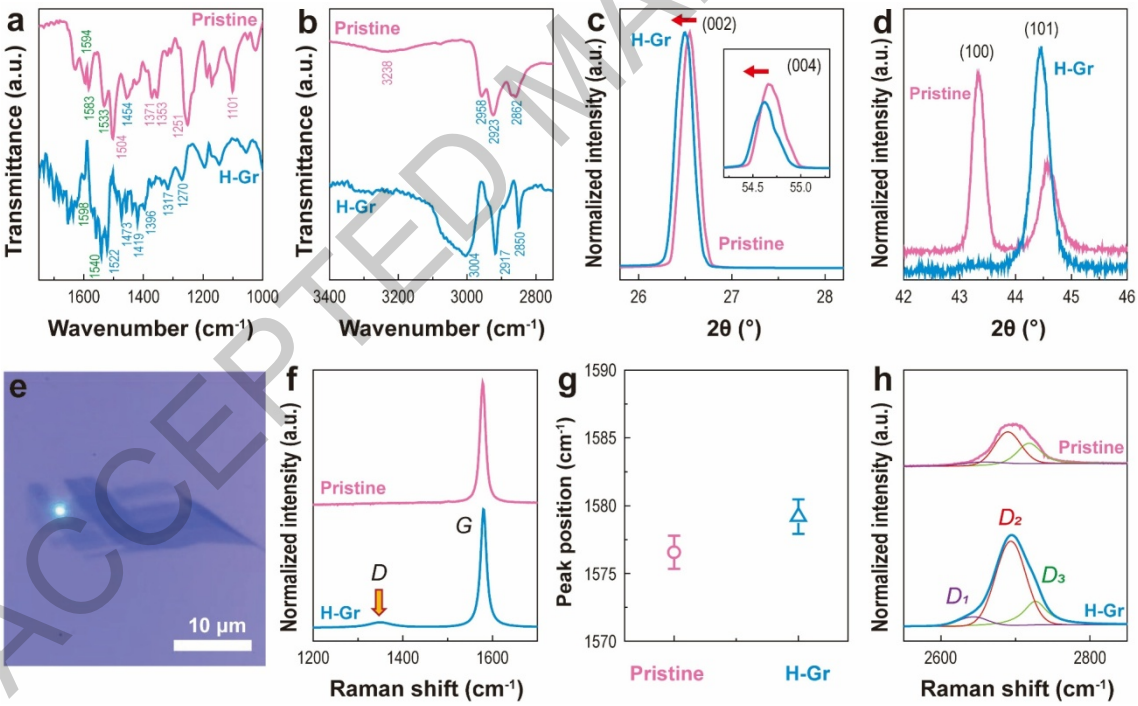

Figure 4. (a)-(b) FT-IR spectra of pristine (pink lines) and H-Gr (hydrogenated graphite powder, blue lines). (c)-(d) XRD patterns of pristine (pink lines) and hydrogenated HOPG (H-Gr, blue lines), showing diffraction peak shifts toward lower angles in H-Gr (red arrows). (e) Optical image of mechanically exfoliated MLG used for Raman spectroscopy. (f) Raman spectra in the *D*- and *G*- band regions for pristine (pink line)

and hydrogenated MLG (H-Gr, blue line), obtained from the position marked in (e). (g) Peak positions of the averaged *G* band for pristine (pink circle) and hydrogenated MLGs (H-Gr, blue triangle), obtained from the eight points shown in Figure 4(e), Figure S9(a), and Figure S10. (h) Variation of *2D* band of pristine (pink line) and hydrogenated MLG (H-Gr, blue line), measured the position marked in (e).

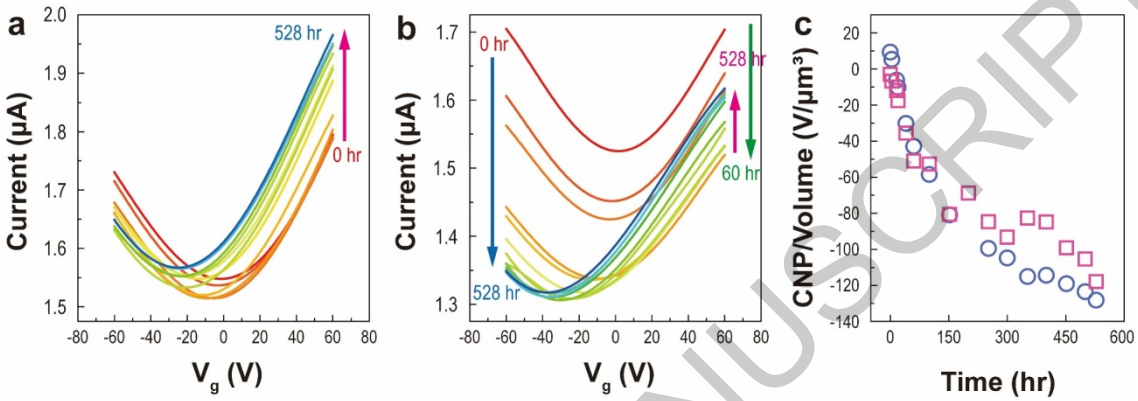

Figure 5. Time-dependent transfer curves of (a) s-MLG and (b) MLG-b at 300 K/80 bar. (c) Change in CNP per volume of s-MLG (pink squares) and MLG-b (blue circles)

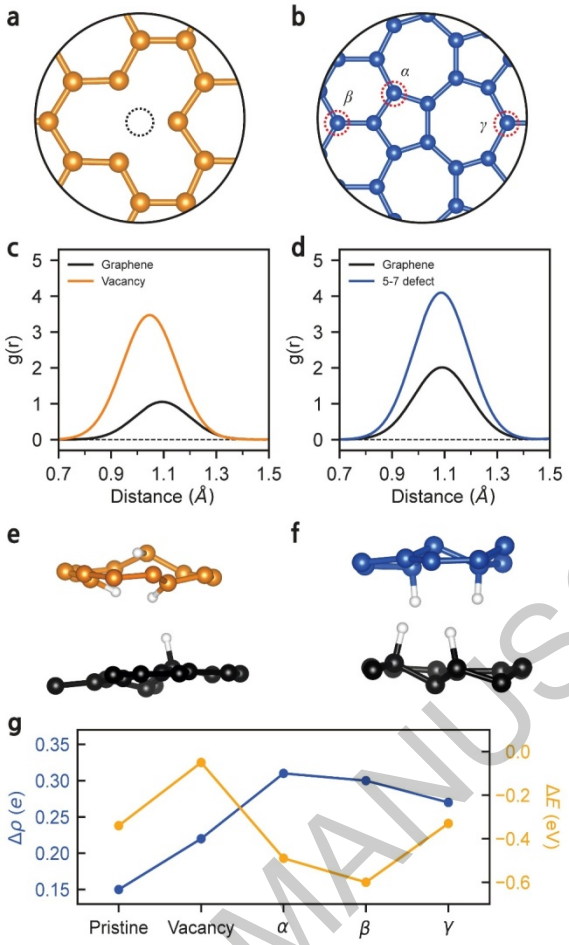

Figure 6. MD simulations of hydrogenated stacked graphene. Atomic structures of (a) single vacancy defect (orange) and (b) 5–7 defects (blue). Three distinct adsorption sites are represented as α, β, and γ. RDF of graphene containing (c) a vacancy or (d) 5–7 defects in a hydrogen environment. The atomic positions are averaged over 0.2 ps after hydrogen adsorption. (e)-(f) Snapshots of hydrogenated graphene layers. Hydrogen adsorption at the defective layer (orange/blue) induces subsequent hydrogen adsorption in the adjacent pristine graphene layer (black). (g) Variation in charge density (blue) and average energy of occupied carbon states (orange) upon hydrogenation for pristine, vacancy, and 5–7 defect (α-γ) layers

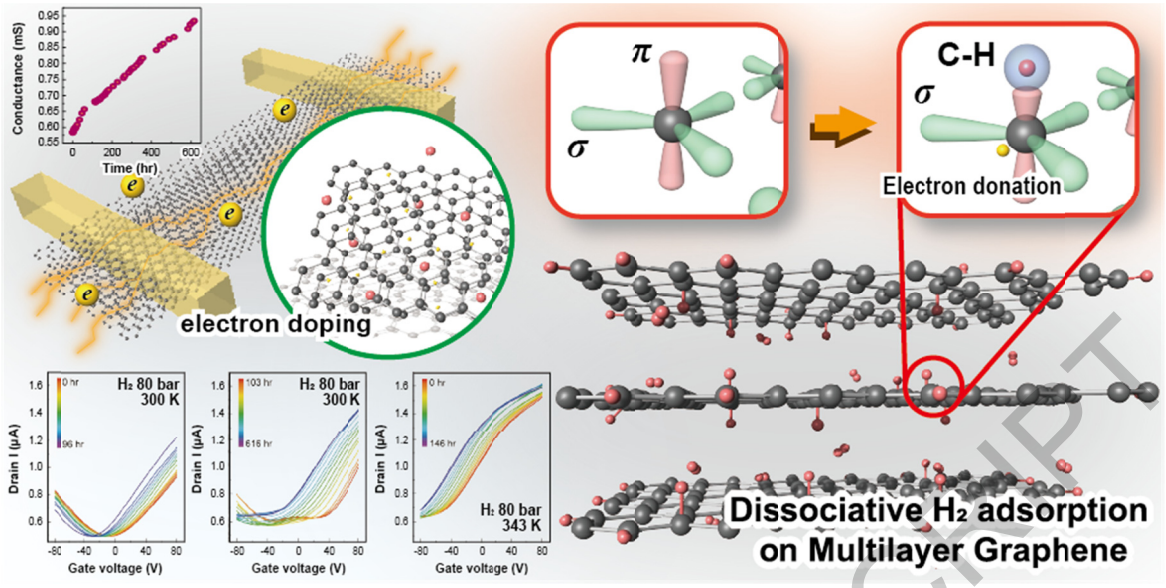

Graphical abstract

IMPACT STATEMENT

This study demonstrates significant electron doping in multilayer graphene through prolonged exposure to high-pressure hydrogen gas, revealing a straightforward method for modifying its electronic properties without harmful chemicals.